Novel Flapping Wing Micro Aerial Vehicle Design Featuring a Bio-inspired Abdomen Mechanism

Jiaxun Leng*, Yuk Wa Steven Ng*, Shun Tang*
info.fwmav@gmail.com
Imperial College London, South Kensington, London

[1]

ABSTRACT

This paper introduces a novel flapping wing micro aerial vehicle (FWMAV) design that integrates a bio-inspired abdomen mechanism to enhance flight stability and maneuverability. By mimicking the abdominal mechanism observed in insects like hawkmoths, our design aims to leverage the abdomen's ability to act as an aerodynamic rudder, shifting the center of mass and redirecting lift forces to achieve instant control responses. The proposed model combines an upper X-wing configuration with a servo-actuated abdomen housing the majority of the vehicle's electronics. This paper will present the equation of motions derived from the Euler-Lagrange Equation and the abdomen's stability properties, followed by experimentally measured data from a computer vision velocity tracking setup and a simulation model to act as a proof of concept and explore the response of the model realistically. This novel design has the potential to significantly improve the performance of FWMAVs in dynamic and unpredictable environments.

1 INTRODUCTION

Bio-inspired flapping wing micro air vehicle (FWMAV) has slowly gained research interest in the MAV community and a few general configurations of FWMAV prototypes have emerged such as the two-wing hummingbird-like configuration[1], X-Wing configuration[2] and tailless configuration[3][4]. However, there still exists a major trade-off between general stability and maneuverability. Recent studies of passive stability and efficient control mechanisms for insect flight might have shined some new light on the issue. The inherently unstable nature of flapping-wing flight can be actively controlled through rapid reactions or passively stabilised with high body drag[5]. Computational studies highlight the complexity of nonlinear interactions affecting stability[6]. The integration of aerodynamics, sensing, and control in insect-scale flapping-wing flight is crucial for achieving stability[7]. Research on the longitudinal dynamic flight stability of insects such as hoverflies and craneflies emphasise the critical role of parts other than the control surfaces[8], particularly the abdomen, in passive stabilisation[9], especially in gusty conditions[10], and hidden stabilisation mechanisms like vibrational control are essential for this process[11]. Traditional approaches often rely on wing stroke plane modulation or the integration of fixed control surfaces to achieve the desired stability. For instance, Nguyen and Chan (2018) developed a tailless FWMAV that utilised wing stroke plane modulation to control flight dynamics, demonstrating effectiveness but at the cost of increased drag each time the status of the wing changes[4]. Similarly, Karasek et al. (2018) explored the use of torque coupling in rapid banked turns, relying heavily on fixed aerodynamic surfaces, which also introduced additional drag and reduced overall efficiency each time the control is activated[3]. De Wagter et al. (2014) emphasized that conventional control surfaces, though functional, can be a limiting factor in achieving optimal flight efficiency in small-scale aerial vehicles[2].

The abdomen of some insects, however, can be one of the pivotal roles not only in maintaining flight stability, especially under gusty conditions but also in maneuverability by acting as an aerodynamic rudder that shifts the centre of mass and redirects lift forces[9]. Recent studies have shown that the hawkmoth (Manduca sexta) uses its abdomen to achieve pitch stability through fine-tuned adjustments that are synchronized with wing beats[10]. The abdominal control mechanisms in moths are crucial for maintaining stable hovering flight, and operating near the edge of stability for quick transitions[10]. Incorporating these insights into the design of flapping wing MAVs can significantly enhance their stability and gust resistance.

This research proposes and demonstrates the

[1] All authors contributed to this work equally and are ranked based on alphabetical order

effectiveness of the novel abdomen control both in flight stability as well as manoeuvrability achieved through centre of mass shifting but also opens new avenues to explore for bio-inspired control algorithms, such as the vibrational control particularly leveraging the active role of the abdomen in enhancing stability. The paper is broken down into three main parts: the first part introduces the mechanical design and actuation of the abdomen; second part introduces the equation of motions of the FWMAV. Finally, the experimental and simulation setup is introduced, where explains our planned experiments and data acquisition.

2 THE DESIGN CONCEPT

The prototype features an upper body of an X-wing configuration with an abdomen lower body, which hosts the electronics that accounts for 65% of the bodyweight. The wing and flapping mechanism follows the same principles as many established works [2][12] and the aerodynamic performance is well documented [13].The FWMAV weighs 40 grams with a wingspan of 33 cm and a body length of 30 cm, dimensions carefully chosen to balance aerodynamic performance and structural integrity. The wing flapping mechanism is capable of achieving a flap angle of 105 degrees, enabling significant lift and thrust generation. The loaded frequency was optimised to 13 Hz to accommodate the aerodynamic forces experienced during flight.

The abdomen part of the model can have potential advantages over the conventional flapping wing drones by dynamically adjusting the position of centre of gravity (CG), providing an additional degree of freedom in the control design. The servo control would also allow for the ability to fine-tune the CG for better control. This is particularly beneficial for flapping wing drones, where quick manoeuvres are often necessary to maintain stability and avoid obstacles such as in urban areas or forests where there is higher density of obstacles. Traditional fixed-wing aircraft can introduce drag. The adjustable abdomen removes the dependency on these surfaces, potentially leading to more efficient flight dynamics with less drag.

2.1 The Abdomen Mechanism

Inspired by the anatomical structure of an insect's abdomen, a mechanism was designed to translate the rotary motion of two servo motors into the rotation of the MAV's abdomen about the pitch and roll axes, which are offset by 12.5 mm. This design effectively decouples the two axes, ensuring that motion in one axis does not interfere with the other. The servos, which are the heaviest individual components of the MAV, are strategically positioned at the bottommost part of the abdomen. This placement, along with any additional electronics, serves to lower the overall center of gravity.

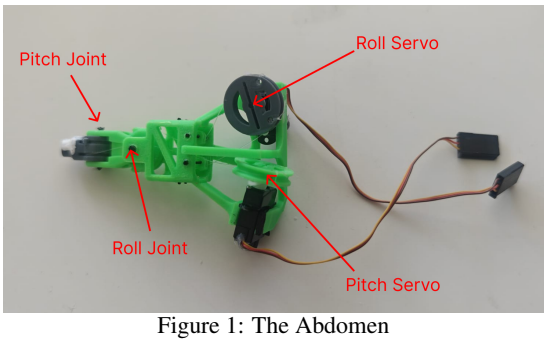

Figure 1: The Abdomen

Lowering the center of gravity confers several advantages to the flapping-wing drone. It enhances the MAV's overall stability, particularly by reducing its propensity for tipping or oscillation during flight, especially in turbulent conditions. Moreover, the lower center of gravity improves control responsiveness, enabling more precise maneuvering and reducing the likelihood of chaotic or unpredictable movements. This stabilization is particularly beneficial during hovering and low-speed flight, contributing to the MAV's overall performance efficiency and stability.

3 FLIGHT DYNAMICS

To demonstrate the effectiveness of the adjustable abdomen control system, it is essential to analyse the dynamic response to abdomen movement. Due to the highly nonlinear nature of the dynamics of FWMAV, the following assumption are made to simplify the model and only retain the most essential and relevant dynamics:

- Longitudinal and lateral dynamics are decoupled and in our model, only the longitudinal dynamics are considered to capture the pitch performance enabled by the abdomen.
- The initial equilibrium condition of the FWMAV is set to be hover.
- The upper and lower body of the FWMAV are modeled as two concentrated masses on massless rigid rods connected by an actuated joint.

3.1 Equation of Motion

The equation of motion is derived using the Lagrange-Euler approach. The dynamic is captured by two pendulums namely, the upper body, and the abdomen body, both of which rotate about the abdomen joint, and the overall system, featuring translational and rotational degree of freedom. The two masses m_1 and m_2 are attached to the ends of two rods of lengths l_1 and l_2 meaning upper body and abdomen respectively. The rods

are assumed to be massless and rigid, and the system is subject to gravity.

Consider first a 2D problem in the longitudinal direction for a generic FWMAV: the undulating of the body is described by angular displacements θ_1 for the upper body and θ_2 for the abdomen. The aerodynamic forces and moments acts on the quarter point of the thorax. Five degrees of freedom were identified and illustrated in Figure 2

- x: Horizontal position of the joint.
- z: Vertical position of the joint.
- θ_t: Angular displacement of the thorax.
- θ_a: Angular displacement of the abdomen.
- θ_0: Pitch angle of the body with respect to the vertical axis.

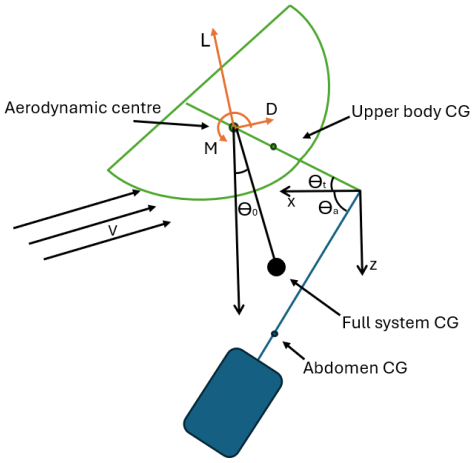

Figure 2: Free body diagram of the FWMAV in a generic condition

3.1.1 Kinetic and Potential Energy

To start with, Euler-Lagrange equations for the system are derived from the Lagrangian $L = T - V$:

$$\frac{d}{dt}\left(\frac{\partial L}{\partial \dot{\theta}_i}\right) - \frac{\partial L}{\partial \theta_i} = 0 \tag{1}$$

The kinetic energy T of the system is:

$$T = \frac{1}{2}m_1\left(\dot{y}_1^2 + \dot{z}_1^2\right) + \frac{1}{2}m_2\left(\dot{y}_2^2 + \dot{z}_2^2\right) \tag{2}$$

The potential energy V includes gravitational potential energy and additional potential energy related to the pitch angle similar to a pendulum hanging from the aerodynamic center. Note that the pitch angle is assumed to be small and therefore small angle approximation applies. This is a valid assumption because we are mostly concerned with small perturbations around the equilibrium point, in this case, hovering:

$$\begin{aligned} V = m_1 g y_1 + m_2 g y_2 = -m_1 g l_1 \cos\theta_1 \\ -m_2 g(l_1\cos\theta_1 + l_2\cos\theta_2) \end{aligned} \tag{3}$$

The Lagrangian L is:

$$L = T - V \tag{4}$$

$$\begin{aligned} L = \frac{1}{2}(m_1+m_2)l_1^2\dot{\theta}_1^2 + \frac{1}{2}m_2 l_2^2\dot{\theta}_2^2 \\ +m_2 l_1 l_2 \dot{\theta}_1\dot{\theta}_2\cos(\theta_1-\theta_2) \\ +(m_1+m_2)g l_1\cos\theta_1 + m_2 g l_2\cos\theta_2 \end{aligned} \tag{5}$$

The Euler-Lagrange equations give us the equations of motion:

$$\begin{aligned} \frac{d}{dt}\left(\frac{\partial L}{\partial \dot{\theta}_1}\right) - \frac{\partial L}{\partial \theta_1} = 0, \\ \frac{d}{dt}\left(\frac{\partial L}{\partial \dot{\theta}_2}\right) - \frac{\partial L}{\partial \theta_2} = 0 \end{aligned} \tag{6}$$

For θ_1:

$$\begin{aligned} (m_1+m_2)l_1^2\ddot{\theta}_1 + m_2 l_1 l_2\ddot{\theta}_2\cos(\theta_1-\theta_2) \\ +m_2 l_1 l_2\dot{\theta}_2^2\sin(\theta_1-\theta_2) \\ +(m_1+m_2)g l_1\sin\theta_1 = 0 \end{aligned} \tag{7}$$

For θ_2:

$$\begin{aligned} m_2 l_2^2\ddot{\theta}_2 + m_2 l_1 l_2\ddot{\theta}_1\cos(\theta_1-\theta_2) \\ +m_2 l_1 l_2\dot{\theta}_1^2\sin(\theta_1-\theta_2) \\ +m_2 g l_2\sin\theta_2 = 0 \end{aligned} \tag{8}$$

3.1.2 Stability Derivatives and System Matrix

For small perturbations around the downward equilibrium ($\theta_1 = 0$, $\theta_2 = 0$), the linearised equations are:

$$\begin{aligned} (m_1+m_2)l_1\delta\ddot{\theta}_1 + m_2 l_2\delta\ddot{\theta}_2 \\ +(m_1+m_2)g\delta\theta_1 = 0 \end{aligned} \tag{9}$$

$$m_2 l_2\delta\ddot{\theta}_2 + m_2 l_1\delta\ddot{\theta}_1 + m_2 g\delta\theta_2 = 0 \tag{10}$$

The linearised system can be written in state-space form as:

$$\dot{\mathbf{x}} = \mathbf{A}\mathbf{x} \tag{11}$$

where the state vector $\mathbf{x}$ is:

$$\mathbf{x} = \begin{bmatrix} \theta_1 & \theta_2 & \dot{\theta}_1 & \dot{\theta}_2 \end{bmatrix}^T \tag{12}$$

The system matrix $\mathbf{A}$ is:

$$\mathbf{A} = \begin{bmatrix} 0 & 0 & 1 & 0 \\ 0 & 0 & 0 & 1 \\ -\frac{(m_1+m_2)g}{(m_1+m_2)l_1} & 0 & 0 & -\frac{m_2 l_2}{(m_1+m_2)l_1} \\ 0 & -\frac{g}{l_2} & -\frac{l_1}{l_2} & 0 \end{bmatrix}$$

The elements of $\mathbf{A}$ correspond to the stability derivatives Z_{θ_1}, Z_{θ_2},$Z_{\dot{\theta}_1}$,$Z_{\dot{\theta}_2}$. The aerodynamic forces were neglected because this analysis is to simulate a hanging situation of the model subject to disturbance.

To analyse stability, we need the characteristic equation of the system. Assume solutions of the form $\delta\theta_1 = Ae^{\lambda t}$ and $\delta\theta_2 = Be^{\lambda t}$. Substitute these into the linearized equations to find λ:

$$\lambda^2 A = -\frac{m_2 l_2}{(m_1+m_2)l_1}\lambda^2 B - \frac{g}{l_1}A$$

$$\lambda^2 B = -\frac{l_1}{l_2}\lambda^2 A - \frac{g}{l_2}B$$

This yields a system of linear equations that can be expressed as:

$$\begin{bmatrix} \lambda^2 + \frac{g}{l_1} & \frac{m_2 l_2}{(m_1+m_2)l_1}\lambda^2 \\ \frac{l_1}{l_2}\lambda^2 & \lambda^2 + \frac{g}{l_2} \end{bmatrix} \begin{bmatrix} A \\ B \end{bmatrix} = \begin{bmatrix} 0 \\ 0 \end{bmatrix}$$

The determinant of this system must be zero for nontrivial solutions:

$$\left(\lambda^2 + \frac{g}{l_1}\right)\left(\lambda^2 + \frac{g}{l_2}\right) - \frac{m_2 l_2}{(m_1+m_2)l_1} \cdot \frac{l_1}{l_2}\lambda^4 = 0$$

Simplifying gives:

$$\lambda^4 + \lambda^2\left(\frac{g}{l_1} + \frac{g}{l_2}\right) + \frac{g^2}{l_1 l_2} = 0$$

This is a quadratic equation in λ^2:

$$\lambda^2 = -\frac{1}{2}\left(\frac{g}{l_1} + \frac{g}{l_2}\right) \pm \sqrt{\left(\frac{1}{2}\left(\frac{g}{l_1} + \frac{g}{l_2}\right)\right)^2 - \frac{g^2}{l_1 l_2}}$$

Applying this onto the model gives $\lambda^2 > 0$ and λ is real, indicating an exponential decay and a stable system.

3.1.3 Settling Time After a Disturbance

The natural frequencies of the system are:

$$\omega_1 = \sqrt{\frac{g}{l_1}}, \quad \omega_2 = \sqrt{\frac{g}{l_2}} \tag{13}$$

The system is critically damped if the damping is just sufficient to return the system to equilibrium without oscillations. Adding critical damping to the velocity terms:

$$c_1 = 2\sqrt{(m_1+m_2)gl_1}, \quad c_2 = 2\sqrt{m_2 g l_2} \tag{14}$$

The time constants τ for damping are:

$$\tau_1 = \frac{1}{\omega_1}, \quad \tau_2 = \frac{1}{\omega_2} \tag{15}$$

The settling time T_{settle} is approximately:

$$T_{\text{settle}} = 4 \times \max(\tau_1, \tau_2) \tag{16}$$

For the prototype with $l_1 = 0.32\,\text{m}$, $l_2 = 0.1\,\text{m}$, $m_1 = 0.013\,\text{kg}$, $m_2 = 0.007\,\text{kg}$, and $g = 9.81\,\text{m/s}^2$:

$$\omega_1 = \sqrt{\frac{9.81}{0.32}} \approx 5.54\,\text{rad/s} \tag{17}$$

$$\tau_1 = \frac{1}{5.54} \approx 0.18\,\text{s} \tag{18}$$

$$T_{\text{settle}} \approx 0.72\,\text{s} \tag{19}$$

This settling time gives an estimate of the short time it takes for the model to stabilise after a disturbance, indicating its promising stability property.

4 EXPERIMENTAL AND SIMULATION SETUP

This section introduces the experimental setup that tracks and measures the abdomen movement utilising computer vision tracking techniques and high-speed cameras. The experiment is designed to measure the transient response of the MAV induced by instantaneous abdomen actuation in near hover conditions and thus characterise the pitch angle control by abdomen actuation.

4.1 Physical hardware setup

The dynamics of the MAV was captured using a monocular, high-speed camera system as shown in Figure 3. The hover condition of MAV was assumed to be equivalent to the MAV suspended with a long string, which provides a simulated aerodynamic force under

small angle deviation from equilibrium. The string was designed to be long to minimise damping effect. A step control signal of 90 deg actuation was sent out from an Arduino UNO microcontroller. To record the MAV's dynamic behavior, a Phantom Miro high-speed camera was positioned perpendicular to the plane of pitch rotation, operating at a frame rate of 1000 frames per second.

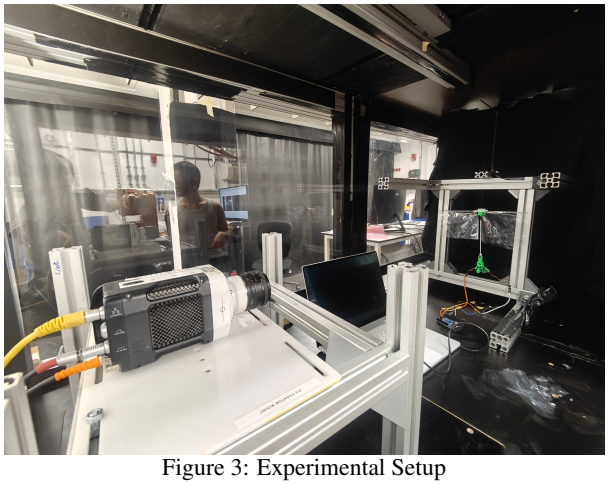

Figure 3: Experimental Setup

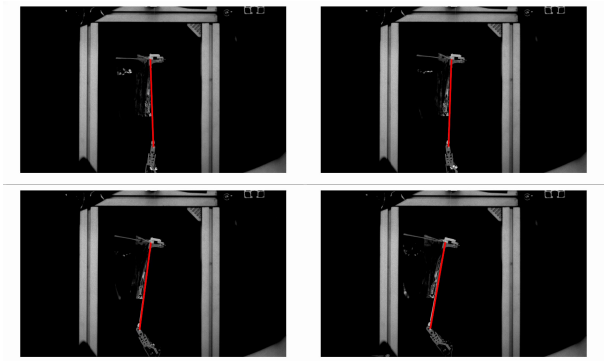

Figure 4: Composite frames taken from high speed footage

4.2 Computer vision powered velocity tracking system

A computer vision algorithm was deployed to process the images and characterize the dynamics of the MAV. The analysis begins by designating the first frame of each video sequence as the reference frame, against which the angular displacement of the MAV's upper body in all subsequent frames is calculated. This method allows for accurate tracking of rotational dynamics over time. Regions of Interest are employed to isolate the MAV's upper body within the video frames to optimize computational efficiency.

Feature tracking was achieved using the MinEigenFeatures method, which detects stable and distinctive points on the MAV's upper body by analyzing the minimum eigenvalue of gradient matrices within the image. These features, identified in the reference frame, are consistently tracked across subsequent frames, enabling precise measurement of the MAV's angular displacement.

To mitigate potential inaccuracies due to video noise and artifacts, the Savitzky-Golay filter is applied as a noise reduction technique. This filter smooths the data while preserving essential features such as peaks and rotational transitions, thereby enhancing the reliability of the calculated angular displacements. Collectively, these computer vision techniques enable precise and reliable characterization of the MAV's dynamic behavior under experimental conditions.

4.2.1 Simulation Setup

Meanwhile, a simulation of the MAV was conducted using the Webots platform to complement the experiment and compared with the experimental results. Instead of using the previously derived simplified model, the simulation was created with the in-built high fidelity physics engine in Webot, capturing the geometrical and dynamical properties more accurately. The simulation environment was set up with all relevant physical properties precisely defined, including the MAV's weight, center of gravity, and detailed physical geometries. These parameters ensure that the virtual model closely mirrors the MAV, providing a reliable foundation for dynamic analysis and will be subsequently used for research in the control algorithm.

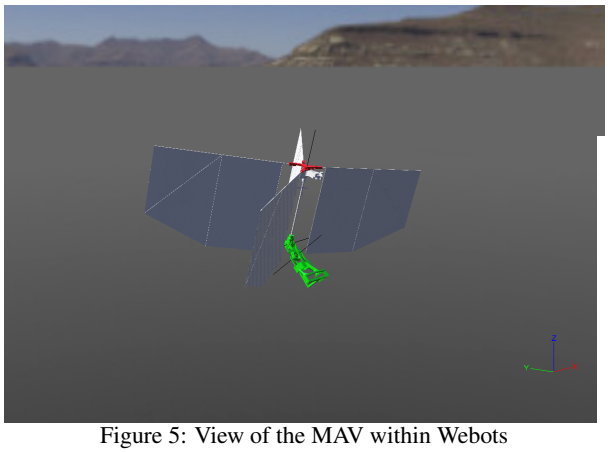

Figure 5: View of the MAV within Webots

Since we are only interested in the near hover condition of the model, the aerodynamic model was simplified and represented by a varying thrust along the direction of the upper body. The unsteady lift in a flapping cycle was setup with experimental data from the wind tunnel testing [13] and was implemented in the model. To achieve near-hover condition in the simulation, the flapping frequency is set to 13Hz. Through iterations, the unsteady lift data was scaled to generate enough thrust to maintain hover condition throughout simulated experiment. The period is set to be 0.0769 seconds as a result of a flapping frequency of 13 Hz accordingly. The aerodynamic centre is assumed to be quarter point of the wing chord and the torque model was derived as shown in the appendix and implemented in the simulation model.

4.3 Results and Discussion

The experiments and simulations conducted in this study provide substantial evidence supporting the effectiveness of the bio-inspired abdomen mechanism in controlling the pitch dynamics of the FWMAV. The results are organized into the following key areas: characterization of the abdomen's impact on pitch control, verification and comparison through simulation.

4.3.1 Characterization of Abdomen Impact on Pitch Control

The experimental setup demonstrated the ability of the abdomen to effectively control the pitch angle of the MAV. By giving an actuation input, we observed a clear and measurable change in the pitch angle, confirming the proposed hypothesis that the abdomen can significantly influence the vehicle's dynamics.

The results are as shown in Figure6: multiple trials with different weight distributions between the body and the abdomen to examine how varying the mass affects the pitch response. The experiments verified the hypothesis that increased abdomen mass or percentage mass over the whole body resulted in a higher pitch angle. This information will be used to inform on the optimal mass allocation minimizing control effort.

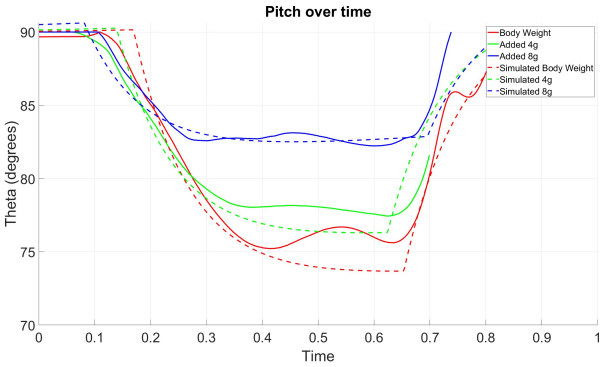

Figure 6: Resulting upper body pitch deflection for Body weight, 4g weight, and 8g weight

4.3.2 Simulation Result Comparison

The simulation results shows consistancy with the experimental data in general validating the simulation model dynamic. As shown in Figure 6, the simulated pitch angles follow the experiment data closely until experimental pitch reached minimum. Then the experimental pitch angle showed increasing rebounce as the abdomen weight increases. This is due to the increasing restoring damping effect of the attached string as the pitch and therefore displacement angle of the string becomes larger, which is what is expected. However, the high degree of correlation between the experimental and simulated results in transient phase in all three cases reinforces the robustness of the simulation model and its potential for further research on the control dynamic of the MAV.

4.3.3 Discussion of Experimental Setup and Assumptions

While the experiments and simulations provided valuable insights, certain assumptions were made in the setup that may affect the generalisability of the results. For instance, the use of a suspended string to simulate hover conditions, while effective, can only be valid in the transient response and unable to capture the full envelope of near hover dynamic. Future studies will need to explore more advanced experimental setups that fully capture the MAV's dynamics in free-flight conditions. Additionally, the linearised equations of motion used in the stability analysis assume small perturbations around the equilibrium point. While this assumption holds for hover conditions, it may not be fully applicable to more dynamic flight scenarios. Further research should explore the full nonlinear dynamics of the MAV

to provide a more comprehensive understanding of its stability and control characteristics.

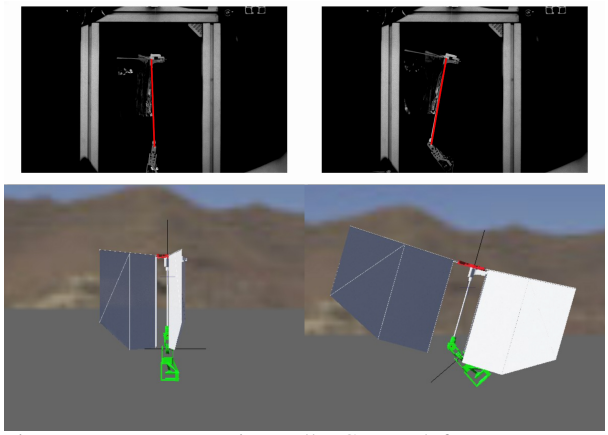

Figure 7: Top: Experimentally Captured frames, Bottom: Simulation

5 CONCLUSION AND FUTURE WORK

This paper introduced a novel flapping wing micro aerial vehicle (FWMAV) with a bio-inspired abdomen mechanism designed to enhance flight stability and maneuverability. Experimental and simulation results confirmed that the abdomen mechanism effectively controls pitch and stabilizes the vehicle by adjusting the center of mass. This bio-inspired approach offers a promising method for achieving agile control in dynamic environments while being passively stable, contributing valuable insights to the design of micro aerial vehicles. Future work will include developing a comprehensive model to explore stability across various flight conditions; conducting experiments in untethered, three-dimensional setups to validate the control mechanisms in realistic scenarios; and using the existing setup to quantify and compare the passive stability as well as maneuverability enabled by abdomen control against the existing control strategies in terms of effectiveness and energy efficiency.

REFERENCES

[1] M. Keennon, K. Klingebiel, and H. Won. Development of the nano hummingbird: A tailless fapping wing micro air vehicle. In *50th AIAA Aerospace Sciences Meeting including the New Horizons Forum and Aerospace Exposition*, page 0588, Nashville, Tennessee, 2012. AIAA.

[2] C. De Wagter, S. Tijmons, B. D. W. Remes, and G. C. H. E. De Croon. Autonomous fight of a 20-gram fapping wing mav with a 4-gram onboard stereo vision system. In *IEEE International Conference on Robotics and Automation*, pages 4982–4987. IEEE, 2014.

[3] M. Karasek, F. T. Muijres, C. De Wagter, B. D. W. Remes, and G. C. H. E. De Croon. A tailless aerial robotic fapper reveals that fies use torque coupling in rapid banked turns. *Science*, 361:1089, 2018.

[4] Q. V. Nguyen and W. L. Chan. Development and fight performance of a biologically-inspired tailless fapping-wing micro air vehicle with wing stroke plane modulation. *Bioinspiration & Biomimetics*, 14:016015, 2018.

[5] Graham K. Taylor and Adrian L. R. Thomas. Active and passive stabilization of body pitch in insect flight. *Journal of The Royal Society Interface*, 10(88):20130237, 2013.

[6] Mao Sun. Aerodynamic performance and stability of insect-inspired flights with. *TLA*, 195:1–10, 2019.

[7] Wei Shyy, Hikaru Aono, Srinath K. Chimakurthi, and Patrick Trizila. Aerodynamics, sensing and control of insect-scale flapping-wing flight. *Journal of the Royal Society Interface*, 10(86):20130297, 2014.

[8] Mao Sun and Yan Xiong. Dynamic flight stability of hovering insects. *Acta Mechanica Sinica*, 23(6):635–647, 2007.

[9] Jonathan P. Dyhr, Kristi A. Morgansen, Thomas L. Daniel, and Noah J. Cowan. Flexible strategies for flight control: an active role for the abdomen. *Journal of Experimental Biology*, 216(9):1523–1536, 2013.

[10] Noah J. Cowan, Kristi A. Morgansen, Thomas L. Daniel, and Jonathan P. Dyhr. Model predictive control of abdominal movements for flight stability in hovering moths. *IEEE Transactions on Robotics*, 30(4):853–864, 2014.

[11] Ralph A. DiCaprio and Noah J. Cowan. Vibrational control: A hidden stabilization mechanism in insect flight. *Science Robotics*, 5(48):eabb1502, 2020.

[12] Quoc-Viet Nguyen, Woei Leong Chan, and Marco Debiasi. An insect-inspired flapping wing micro air vehicle with double wing clap-fling effects and capability of sustained hovering. In *Bioinspiration, Biomimetics, and Bioreplication 2015, edited by Akhlesh Lakhtakia, Mato Knez, Raúl J. Martín-Palma*, page 94290U. SPIE, 2015.

[13] S. F. Armanini, J. V. Caetano, G. C. H. E. de Croon, C. C. de Visser, and M. Mulder. Quasi-steady aerodynamic model of clap-and-fling flapping mav and validation using free-flight data. In *AIAA*

Atmospheric Flight Mechanics Conference. AIAA, 2016.

APPENDIX

.1 Derivation of abdomen torque model

To model the relationship between torque and angular position for the servo-actuated abdomen joint, we define the following system parameters for a typical DC servo motor:

- R: Resistance of the motor windings (Ohms)
- L: Inductance of the motor windings (Henrys)
- K_e: Back EMF constant (V/(rad/s))
- K_t: Torque constant (Nm/A)
- J: Moment of inertia (kg m^2)
- B: Damping coefficient (Nm/(rad/s))

The voltage equation for the motor and the torque produced by the motor are respectively:

$$V(t) = I(t)R + L\frac{dI(t)}{dt} + K_e\omega(t)$$

$$\tau(t) = K_t I(t)$$

$$\tau(t) = J\frac{d\omega(t)}{dt} + B\omega(t)$$

we can easily get:

$$V(t) = \frac{LJ}{K_t}\frac{d^2\omega(t)}{dt^2} + \left(\frac{JR}{K_t} + \frac{LB}{K_t}\right)\frac{d\omega(t)}{dt} + \left(\frac{BR}{K_t} + K_e\right)\omega(t)$$

.1.1 Torque as a Function of Angular Position

The torque function derived earlier is:

$$\tau(t) = \frac{K_t}{R}V(t) - \frac{LJ}{R}\omega''(t) - \left(J + \frac{LB}{R}\right)\omega'(t) - \left(B + \frac{K_e}{R}\right)\omega(t)$$

In the Laplace domain, substituting $V(s) = (as^2 + bs + c)\Theta(s)$ into the torque function and simply we get:

$$\tau(s) = \left(\frac{K_t LJ}{RK_t} - \frac{LJ}{R} - \frac{RJ}{R} - \frac{LB}{R}\right)s^2\Theta(s) + \left(\frac{K_t\left(\frac{JR}{K_t} + \frac{LB}{K_t}\right)}{R} - \frac{B + K_e}{R}\right)s\Theta(s) + \frac{K_t\left(\frac{BR}{K_t} + K_e\right)}{R}\Theta(s)$$

Let:

$$A = \frac{K_t a - LJ - RJ - LB}{R}$$

$$B = \frac{K_t\left(\frac{JR}{K_t} + \frac{LB}{K_t}\right) - B - K_e}{R}$$

$$C = \frac{K_t\left(\frac{BR}{K_t} + K_e\right)}{R}$$

Hence, the torque in terms of the angular position in the Laplace domain is as follow and a transfer function relating torque produced to angular position of the motor given an actuation command is derived.

$$\tau(s) = \left(As^2 + Bs + C\right)\Theta(s) \tag{20}$$

.1.2 Servo Control

A regular servo typically actuates from point A to point B at a constant speed. However, this constant speed can introduce a sudden impulse or jerk, particularly in delicate mechanisms like flapping-wing micro aerial vehicles (FWMAVs). This jerking motion can negatively impact the stability and performance of the MAV. To address this issue, velocity control strategies were implemented to smooth the transition between positions, thereby reducing the jerk and enhancing the overall stability and performance of the MAV.

The goal is to transition the servo from the initial angle α to the objective angle β within a specified actuation time T, in a manner that minimizes jerk. This was achieved by controlling the velocity profile of the servo.

$$a0 = \alpha$$

$$a1 = \frac{3}{T^2}\cdot(\beta - \alpha)$$

$$a2 = -\frac{2}{T^3}\cdot(\beta - \alpha)$$

Where:

- $a0$, $a1$, and $a2$ are coefficients that define the polynomial for the position $\theta(t)$ over time.
- α is the initial angle.
- β is the objective angle.
- T is the total time of actuation.
- t is the current time step.

The position $\theta(t)$ of the servo at any given time t is described by the cubic polynomial:

$$\theta(t) = a0 + a1 \cdot t^2 + a2 \cdot t^3$$

This polynomial ensures a smooth transition from α to β over the time T.

1. Initial Conditions:
   (a) At $t = 0$, $\theta(0) = \alpha$. Thus, $a0 = \alpha$.
   (b) At $t = T$, $\theta(T) = \beta$.
2. Velocity Constraints:
   (a) The initial velocity and final velocity is zero, ensuring smooth stop.
3. Jerk minimization:
   (a) The cubic polynomial $\theta(t) = a0 + a1 \cdot t^2 + a2 \cdot t^3$ is chosen to ensure continuous acceleration and to minimize jerk.